Int. J. Multiphase Flow Vol. 6, pp. 499–521
Pergamon/Elsevier, 1980. Printed in Great Britain

A GENERAL MODEL FOR UNCONFINED BUBBLE PLUMES FROM EXTENDED SOURCES

A. K. CHESTERS†, M. VAN DOORN‡ and L. H. J. GOOSSENS‡
Delft University of Technology, Delft, The Netherlands

(*Received* 20 *May* 1978; *in revised form* 25 *April* 1980)

Abstract—A model for unconfined bubble plumes is developed without assumptions as to the form of the velocity and gas-fraction profiles or as to the fraction of the momentum flux associated with the mean flow. Dimensionless solutions for axisymmetric and plane-symmetric extended sources indicate an initial contraction followed by an almost linear expansion which closely resembles the single-phase case. A second contraction is predicted near the surface of deep bodies of liquid. Gas and liquid velocity measurements in laboratory-scale plumes are presented, providing information on entrainment coefficients, velocity profiles, bubble velocities and the contribution of velocity fluctutations to the total momentum flux. The latter effect is considerable, providing an explanation of the "too-low" plume velocities found by other investigators.

1. INTRODUCTION

The upward flow ("plume") produced by the continuous injection of gas in a body of liquid has many important applications, aside from its intrinsic interest: destratification of reservoirs, prevention of salt intrusion in harbours, mixing in steelmaking processes, and so on. Practical situations may be divided into the unconfined case, in which the width of the body of liquid is large in comparison with that of the plume, and the confined case in which this is not so. In what follows, attention is restricted to the unconfined case, for which the pressure variation outside the plume is approximately hydrostatic. The confined case has been considered by Freedman & Davidson (1969) and Rietema & Ottengraf (1970).

The unconfined case has already received considerable attention: Cederwall & Ditmars (1970), Abraham (1972), Kobus (1973, summarizing earlier work), Goossens & Smith (1975), Hussain & Siegel (1976), Tekeli & Maxwell (1978), the others. Only three of the above investigations included measurements: Kobus and Goossens & Smith (liquid-velocity measurements with a propeller), and Tekeli & Maxwell (hot-wire measurements of liquid velocity, gas fraction and bubble velocity). In developing their theories, all investigators:

(i) Made specific assumptions as to the form of the (mean) liquid-velocity and gas-fraction profiles (top-hat in the case of Hussain and Siegel, Gaussian in the other cases).

(ii) Ignored contributions to the momentum flux of the plume from the fluctuating component of the liquid velocity.

(iii) Made simplifying assumptions as to the initial development of the plume and the influence of injection geometry—usually the assumption of a virtual origin of (*a priori*) unknown location.

The present contribution is both theoretical and experimental. On the theoretical side, attention is directed to the above three points. Plume equations are developed without assumptions as to the form of the liquid-velocity or gas-fraction profiles or as to the proportion of the total momentum flux associated with the mean flow. The influence of injection geometry on initial and later plume development is investigated for the case of extended sources (perforated discs or strips). The plume is predicted to undergo an initial contraction (later confirmed experimentally). A second contraction, not yet observed, is predicted near the surface of deep bodies of liquid. Finally, a new method of normalizing the plume equations is introduced based on the primary parameters of influence: gas injection rate and acceleration

†Laboratory of Aero- and Hydrodynamics.
‡Laboratory of Physical Technology.

due to gravity. The dimensionless characteristics of large and small, single and two-phase plumes are then seen to be surprisingly similar.

On the experimental side, local measurements are presented of mean liquid velocity (laser-doppler anemometry) and bubble velocity (double-electrode method) in small plumes from axisymmetric extended sources. Unlike the results of Tekeli and Maxwell, relative bubble velocities are found to agree with free-rise values. The liquid-velocity measurements lead to the conclusion that a considerable proportion (sometimes more than half) of the total momentum flux of the plume is associated with the fluctuating component of the liquid velocity. This effect, which appears to be correlated with the stirring action of the bubbles, is probably the cause of the "too-low" plume velocities noted by various other investigators (Cederwall & Ditmars1970, Tekeli & Maxwell 1978). Mass entrainment rates of the plumes investigated are found to be close to, or slightly greater than, those of single-phase free jets/buoyant plumes.

2. DERIVATION OF THE PLUME EQUATIONS

2.1 *Qualitative basis*

The situation to be considered is depicted in figure 1. Three stages in the evolution of the flow may be distinguished.

(1) Close to the gas-injection plane the liquid has no vertical motion except in the immediate vicinity of individual bubbles.

(2) This wake liquid shares its momentum with adjacent liquid and at some critical height all the liquid between the bubbles is in upward motion. This marks the beginning of the second stage, in which the flow may be considered to be a "plume".

(3) The plume reaches the surface and the liquid flows off horizontally.

In what follows, attention is focussed on stage 2. Stage 1 is considered briefly to establish the initial conditions for stage 2, but is concluded to be very short-lived in general.

The evolution of the plume from its initial condition is determined by the rate of increase of its momentum flux, M, due to buoyancy and of its mass flux, m, due to entrainment. Momentum increase alone leads to contraction of the plume (as in a slow stream of water from a tap), increase of mass flux alone to expansion (as in a free non-buoyant yet). Which of these two processes dominates depends on the region of the plume concerned (figure 13).

It is important to note that the mean momentum flux, M, is given by (axisymmetric case)

$$M = \rho \int_0^\infty 2\pi r(1-\alpha)\overline{u^2}\,\mathrm{d}r \qquad [1]$$

$$= \bar{M} + \tilde{M}, \qquad [2]$$

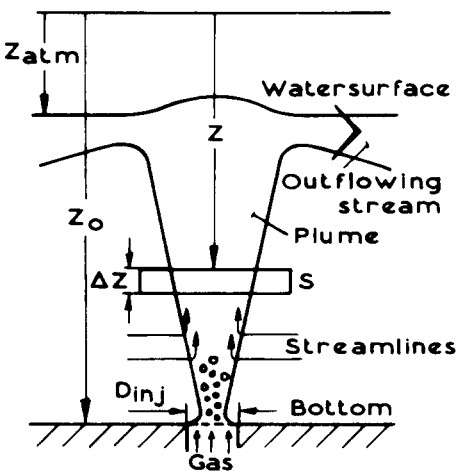

Figure 1. Unconfined bubble plume from an extended source.

where

$$\bar{M} = \rho \int_0^\infty 2\pi r(1-\alpha)(\bar{u})^2 \, dr \qquad [3]$$

and

$$\tilde{M} = \rho \int_0^\infty 2\pi r(1-\alpha)\overline{(\tilde{u})^2} \, dr. \qquad [4]$$

Here r denotes radial distance, ρ liquid density, α the fraction of the time that gas is present in a point, u instantaneous liquid velocity, an overbar an average over the time that liquid is present, and $\tilde{u}$ the instantaneous departure of u from $\bar{u}$. Here and elsewhere the momentum of the gas is neglected. In the case of single-phase, free, turbulent jets ($\alpha = 0$) $\tilde{M}$ is around 10 per cent of $\bar{M}$ and is often disregarded. In the case of two-phase buoyant plumes, however, the two terms may initially be of the same order, leading to the apparent disappearance of momentum if $\bar{M}$ alone is regarded.

2.2 *General momentum-increase equation*

The rate of increase of the momentum flux is readily obtained from a force balance on an element of the plume (that within the control surface S, figure 1) if a number of simplifying approximations are made. Most of these are the same as in the theory of single-phase buoyant plumes (Turner 1969) and will not be repeated here. An additional approximation in the two-phase case is that the extra forces on the upper and lower surfaces of S due to cut bubbles (surface tension forces, excess-pressure forces within the bubbles, excess-pressure and viscous forces in the vicinity of bubbles) cancel. This approximation, like that of constant pressure across the plume, is justified if the expansion/contraction of the plume is sufficiently gradual. The momentum increase of the plume is then given by

$$dM/dz = -\rho g a, \qquad [5]$$

where z is distance measured vertically downward from an origin z_{atm} above the liquid surface, such that

$$\rho g z_{atm} = p_{atm} \qquad [6]$$

(g acceleration due to gravity, p_{atm} atmospheric pressure) and a is the area occupied by gas in a cross section. The density of the gas has been neglected. For the single-phase case, ρ corresponds to the average density difference and a is the cross-sectional area of the plume.

2.3 *General mass-increase equation*

The turbulent entrainment law for single-phase axisymmetric plumes (Turner 1969) is

$$dm/dz = -K\rho v d, \qquad [7]$$

where v and d are measures of the local plume velocity and diameter. In the absence of *a priori* knowledge of the velocity profile v and d may be derived from m and M:

$$m = \rho(\pi d^2/4)v, \quad M = \rho(\pi d^2/4)v^2 \qquad [8], [9]$$

v and d are the "equivalent" velocity and diameter which the plume would have were its

velocity profile square. Equations [8] and [9] yield

$$d = 2m/\sqrt{(\pi\rho M)}\,, \quad v = M/m\,. \qquad [10],[11]$$

Turner (1969) concludes the value of K for single-phase buoyant plumes to be the same within experimental error as that for single-phase free jets: $K \simeq 0.25$ (Ricou & Spalding 1961) for the above choice of v and d.

For a Gaussian profile of velocity with no velocity fluctuations and negligible gas fraction,

$$u = \bar{u} = u_{\max}\, e^{-r^2/b^2}\,, \qquad [12]$$

[10] and [11] yield (Appendix 1)

$$d = 2\sqrt{(2)}b\,, \quad v = u_{\max}/2\,. \qquad [13],[14]$$

A physical interpretation of [7] is that the radial velocity with which matter is entrained is proportional to the plume velocity. The presence of d in the r.h.s. of [7] takes into account the area of the entraining surface. In the two-phase case, this surface is somewhat exetnded for given m and M (and hence given d and v) due to the sectional area, a, occupied by the bubbles. The two-phase analogue of [7] is accordingly written as

$$dm/dz = -K_1\rho v d_{\text{eff}}\,, \qquad [15]$$

where

$$\pi d_{\text{eff}}^2/4 = \pi d^2/4 + K_2 a\,, \qquad [16]$$

and K_2 is a dimensionless parameter of order unity. It is to be expected that

$$K_1 = 0(K) = 0(0.25)\,. \qquad [17]$$

2.4 *Gas-continuity*

The value of a is related to the average gas velocity in the relevant cross section, v_G, by

$$m_G = \rho_G v_G a\,. \qquad [18]$$

For isothermal expansion of the bubbles,

$$\rho_G = (\rho_G)_o z/z_o\,, \qquad [19]$$

(m_G mass injection rate of gas, ρ_G gas density, suffix o: in the injection plane). v_G may be written as

$$v_G = K_3 v + v_r\,. \qquad [20]$$

The first term gives the mean velocity of the liquid in which the bubbles are situated, K_3 being of order unity. v_r is the mean relative velocity of the bubbles in the relevant cross section. Except in the initial region of the plume, where the gas fraction may be high, v_r may be expected to be approximated by the free-rise velocity of a single bubble, though the influence of plume turbulence of course remains. This expectation is confirmed by the experimental results

(section 5.2.2). In the initial contracting region of the plume Korbijn (1977) concluded v_r to be somewhat lower.

In the case of Gaussian profiles of velocity ([12]) and gas fraction,

$$\alpha = \alpha_{max}\, e^{-r^2/(\lambda b)^2}, \qquad [21]$$

with no velocity fluctuations and $\alpha_{max} \ll 1$, it is readily shown (appendix 1) that

$$K_3 = 2/(1+\lambda^2). \qquad [22]$$

Combination of [18]–[20] yields

$$a = G_0 z_0 / z(K_3 v + v_r) \qquad [23]$$

where G_o denotes the volume injection rate of gas, $m_G/(\rho_G)_o$.

2.5 *General plume equations*

Making use of [8], [9], [16] and [23], the momentum and mass equations [5] and [15] yield, on rearrangement, two coupled equations for the variation of d and v with height in the axisymmetric case:

$$\frac{-\mathrm{d}(d)}{\mathrm{d}Z} = [-gG_0 z_0/2z(K_3 v + v_r) + K_1 dv^2\{1 + 4K_2 G_o z_o/\pi d^2 z(K_3 v + v_r)\}^{1/2}]/(\pi d v^2/4). \qquad [24]$$

$$\frac{-\mathrm{d}v}{\mathrm{d}z} = [gG_o z_o/z(K_3 v + v_r) - K_1 dv^2\{1 + 4K_2 G_o z_o/\pi d^2 z(K_3 v + v_r)\}^{1/2}]/(\pi d^2 v/4). \qquad [25]$$

The corresponding equations for the plane-symmetric case prove to be:

$$\frac{-\mathrm{d}(d)}{\mathrm{d}z} = [-gG_o z_o/z(K_3' v + v_r) + 2K_1' v^2]/v^2 \qquad [26]$$

$$\frac{-\mathrm{d}v}{\mathrm{d}z} = [gG_0 z_0/z(K_3' v + v_r) - K_1' v^2]/vd \qquad [27]$$

where the equivalent width d and velocity v of the plume are defined by the equations

$$m = \rho v d, \qquad M = \rho v^2 d \qquad [28], [29]$$

The quantities G_o, m and M are now per unit length of the plume. The expressions are simpler than those for the axisymmetric case since the entrainment law for a plane single-phase plume,

$$\mathrm{d}m/\mathrm{d}z = -K'\rho v, \qquad [30]$$

does not involve d and no use need therefore be made of a d_{eff}. The value of K' is approx. 0.16 (Turner 1969).

The general plume equations [24]–[27] reduce to those of Cederwall and Ditmars if the K_2 term is omitted and the substitutions made appropriate to a Gaussian velocity profile with no velocity fluctuations and $\alpha_{max} \ll 1$ ([13], [14] and [22] in the axisymmetric case, or [A1.6], [A1.7] and [A1.13] in the plane-symmetric case).

2.6 *Asymptotic and normalized plume equations*

To the authors' knowledge, the axisymmetric plume equations [24] and [25] have no analytical solution except in the asymptotic case of:

(i) $v_r \to 0$.
(ii) $z,\ z_o \to \infty,\ z_0/z \to 1$.
(*iii*) $z_o - z$, and hence d, large so that

$$4G_o z_o/\pi d^2 z(K_3 v + v_r), = a/(\pi d^2/4), \ll 1.$$

In this case the equations reduce to

$$\frac{-\mathrm{d}(d)}{\mathrm{d}z} = \frac{-2gG_o}{\pi K_3 d v^3} + \frac{4K_1}{\pi} \qquad [24a]$$

$$\frac{-\mathrm{d}v}{\mathrm{d}z} = \frac{4gG_o}{\pi K_3 d^2 v^2} - \frac{4K_1 v}{\pi d} \qquad [25a]$$

which have the solution

$$d = -(12K_1/5\pi)(z - z_{\text{virt}}), \quad 1/v^3 = -(48K_3K_1^2/25\pi g G_o)(z - z_{\text{virt}}) \qquad [31], [32]$$

where $(z_o - z_{\text{virt}})$ is an unknown constant corresponding to the position of a virtual origin. Equations [31] and [32] correspond, as they should, to the form of solution obtained for incompressible single-phase buoyant plumes (Turner 1969). If the density, ρ_1, of the lighter fluid is no longer negligible, G_o must be replaced by $G_o(\rho_2 - \rho_1)/\rho_2$.

The equations for the plane case corresponding to [31] and [32] are:

$$d = -K_1'(z - z_{\text{virt}}), \quad v = (gG_o/K_3'K_1)^{1/3} = \text{constant}. \qquad [33], [34]$$

In the above situation only two physical parameters remain to determine the plume development: G_o and g. The only characteristic length and velocity scales, L and U, which can be constructed from these are:

$$L = (G_o^2/g)^{1/5}, \quad U = (G_o g)^{1/5} \qquad [35], [36]$$

$$\text{(plane case: } L = (G_o^2/g)^{1/3}, \quad U = (G_0 g)^{1/3}) \qquad [37], [38]$$

These scales can be used to non-dimensionalize the equations and their solutions. The solutions [31]–[34] then become

$$D = (-12K_1/5\pi)(Z - Z_{\text{virt}}), \quad 1/V^3 = -(48K_3K_1^2/25\pi)(Z - Z_{\text{virt}}) \qquad [31'], [32']$$

and

$$D = -K'(Z - Z_{\text{virt}}), \quad V = (K_3'K_1')^{-1/3} \qquad [33'], [34']$$

in which capital letters denote dimensionless quantities ($D = d/L$, $V = v/U$, etc.).

In the two-phase case, other length and velocity scales are also impressed – z_o, v_r and those connected with the initial conditions and it is not clear *a priori* which are the most suitable for normalizing the plume equations. The results of numerical solutions (section 4.2) indicate that

under conditions of practical interes tthe primary parameters of influence are the same as in the single-phase case, namely G_o and g. z_o, v_r and the initial conditions are of secondary influence and when the two-phase equations are normalized with the help of the scales of [35]–[38], the dimensionless solutions therefore bear a close resemblance for large or small, single- or two-phase plumes and for diverse initial conditions.

Tekeli and Maxwell normalized their equations with the velocity scale of [36] and [38] but used z_o as length scale. Cederwall and Ditmars also chose z_o as length scale and chose $v_r(1+\lambda^2)$ as velocity scale. This has the appeal that the normalized solutions depend on only one† parameter, $K_1(1+\lambda^2)(z_0 v_r^3/gG_0)^{1/2}$. The dimensionless solutions, however, are very sensitive to the value of this parameter, which is to be expected since the scales chosen depend strongly on the values of v_r and z_o whereas the actual plume behaviour does not.

Making use of [35]–[38], the normalized forms of [24]–[27] become: axisymmetric case

$$\frac{-\mathrm{d}D}{\mathrm{d}Z} = [-Z_o/2Z(K_3V+V_r)+K_1DV^2\{1+4K_2Z_o/\pi D^2Z(K_3V+V_r)\}^{1/2}]/(\pi DV^2/4) \qquad [24']$$

$$\frac{-\mathrm{d}V}{\mathrm{d}Z} = [Z_o/Z(K_3V+V_r)-K_1DV^2\{1+4K_2Z_o/\pi D^2Z(K_3V+V_r)\}^{1/2}]/(\pi D^2V/4) \qquad [25']$$

plane-symmetric case

$$\frac{-\mathrm{d}D}{\mathrm{d}Z} = [-Z_o/Z(K_3'V+V_r)+2K_1'V^2]/V^2 \qquad [26']$$

$$\frac{-\mathrm{d}V}{\mathrm{d}Z} = [Z_o/Z(K_3'V+V_r)-K_1'V^2]/VD. \qquad [27']$$

3. INITIAL CONDITIONS

The transition from stage 1 to stage 2 discussed in section 2.1, whereby all the liquid between the bubbles first attains an upward velocity provides the initial conditions for the plume development. In the immediate vicinity of a bubble the liquid then has a velocity of order v_r, while exactly between bubbles the velocity is almost zero. The initial equivalent plume velocity, v_o, may therefore be written as

$$v_o = \beta v_r, \quad \text{or} \quad V_o = \beta V_r, \qquad [39], [39']$$

where $\beta = 0(0.5)$.

The initial value of d_{eff} is equal to the width of the gas-injection device. In the axisymmetric case, therefore,

$$\pi d_{\text{inj}}^2/4 = \pi(d_{\text{eff}})_o^2/4 = \pi d_o^2/4 + K_2 a$$

$$d_o^2 = d_{\text{inj}}^2 - 4K_2G_o/\pi(1+K_3\beta)v_r, \qquad [40]$$

or

$$D_o^2 = D_{\text{inj}}^2 - 4K_2/\pi(1+K_3\beta)V_r, \qquad [40']$$

making use of [16], [39], [23], [40] and the fact that $Z = Z_o$ very nearly (see below). In the

†Two if K_2 is included.

plane-symmetric case the corresponding condition is

$$d_o = d_{\text{inj}} - K_2' G_o/(1 + K_3'\beta) v_r, \qquad [41]$$

or

$$D_o = D_{\text{inj}} - K_2'/(1 + K_3'\beta) V_r \qquad [41']$$

[40] and [41] indicate that if G_o is increased for a given gas-injection device, d_o decreases, finally becoming zero at some critical G_o value. Beyond this point the rise velocity of the bubbles is insufficient to carry off the gas in bubble form and a change in initial flow regime must occur. This new situation is beyond the scope of the present considerations, but is discussed briefly in section 5.1.

The only question remaining is the height above the injector at which the transition from stage 1 to stage 2 occurs. The momentum equation [5] also applies to stage 1, and since no global liquid motion exists, $v_G \sim v_r$, while $z \sim z_o$. [5] therefore yields

$$-\mathrm{d}M/\mathrm{d}z \sim \rho g G_o/v_r, \quad \text{i.e.} \quad -\Delta z \sim \Delta M v_r/\rho g G_o. \qquad [42]$$

At the transition to stage 2,

$$\Delta M = M = \rho(\pi d_o^2/4)(\beta v_r)^2$$

and [42] becomes

$$-\Delta z \sim \pi\beta^2 d_o^2 v_r^3/4gG_o, \quad \text{or} \quad -\Delta Z \sim \pi\beta^2 D_o^2 V_r^3/4. \qquad [43], [43']$$

For the values of D_o and V_r of practical interest (section 4.1), it will be seen that

$$-\Delta Z \leqslant 1$$

so that the height of the stage 1 zone may in general be neglected and the plume development approximated as commencing immediately above the gas injector.

4. NUMERICAL SOLUTIONS OF THE DIMENSIONLESS PLUME EQUATIONS

4.1 *Range of paremeters of practical interest*

The range of values of the various parameters of practical interest in the axisymmetric case is indicated in Table 1. G_o ranges from the order of $10^{-4}\,\mathrm{m^3\,s^{-1}}$ ($L = 1.6\,\mathrm{cm}$, $U = 0.4\,\mathrm{m\,s^{-1}}$) in small laboratory plumes to the order of $10^{-1}\,\mathrm{m^3\,s^{-1}}$ ($L = 25\,\mathrm{cm}$, $U = 1.6\,\mathrm{m\,s^{-1}}$) in, for example, a natural-gas blow-out under the North Sea. The corresponding range of Z_o values is comparatively narrow however since, as in the above examples, large G_o values are generally accompanied by large depths of liquid.

Table 1. Range of parameters in the axisymmetric case

Parameter	Min.	Max.	Standard
Z_o	10^2	10^3	500
V_r	0.125	0.5	0.25
D_o	0.5	10	2

The free-rise velocity of bubbles in water in the most usual size range of a few mm to a few cm varies little (20–30 cm/s) and the tabulated variation of V_r is largely a reflection of the variation in U.

The wide range of D_o values reflects the fact that there is little practical limitation on this value.

A similar range is to be expected in the plane-symmetric case.

4.2 *Results*

The dimensionless plume equations for the axisymmetric case, [24] and [25], are readily integrated in parallel by a simple finite-difference scheme. The variation of D and V with height is presented in figures 2 and 3 for the "standard" case (table 2). The related values of D_{eff}, of the dimensionless sectional area occupied by gas and of the dimensionless mass and momentum fluxes are obtainable from the dimensionless forms of the relations [23], [16], [8] and [9].

The plume is seen first to undergo a contraction, after which it expands until $Z \sim D$, when a second contraction occurs. This behaviour is qualitatively explicable as follows. The increase in momentum of the plume with height tends to increase its velocity and hence, by continuity, decrease its diameter. Mass entrainment has the opposite effect. Initially the latter process is

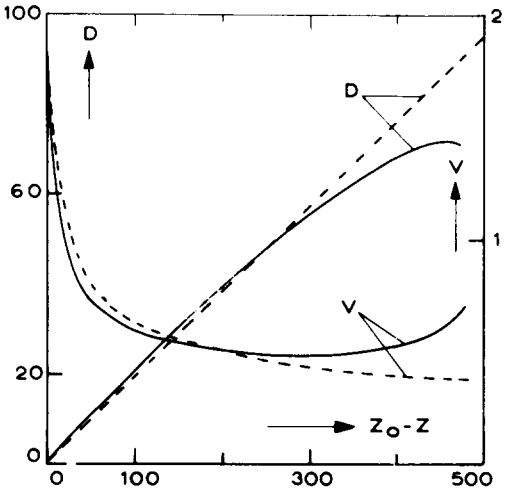

Figure 2. Variation of D and V with height in the standard axisymmetric case (the broken lines indicate the asymptotic solution).

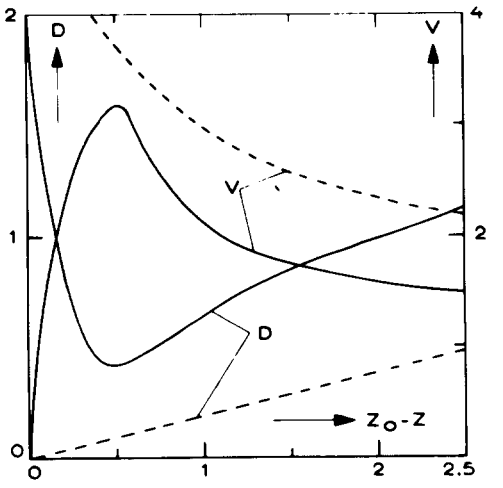

Figure 3. As figure 2. Initial development of the plume.

Table 2. Standard values of the various parameters in the axisymmetric case

Parameter	Standard value
Z_o	500
V_r	0.25
D_o	2
β	0.5
K_1	0.25†
K_2	1
K_3	1

†Single-phase free jet/plume

weak because of the low plume velocity but the former is not: hence the initial contraction. Later, mass entrainment is the stronger effect and the plume velocity decreases while its diameter increases. When Z (and hence the absolute pressure) becomes very small, however, the volume of buoyant gas becomes very large and the momentum increase again dominates, leading to a second contraction. For this contraction to be observable, the liquid depth would have to be some $20\, z_{atm}$, a condition which is only satisfied in the sea or in low-pressure systems. This explains the absence of observation of the effect.

During the expansion phase of the plume, up to $Z \sim Z_o/3$, the variation of D is closely approximated by the asymptotic solution, in which the virtual origin has for simplicity been chosen in the plane of injection. V is initially somewhat lower than in the asymptotic case, as would be expected from the non-zero value of v_r (smaller α, less buoyancy) but catches up at $Z \sim Z_o/3$ due to the increased volume of gas. This close similarity to the asymptotic (i.e. single-phase plume) solution will be seen to be maintained if the various parameters are assigned other values (figures 4–10).

The influence of the β and K_2 values (figures 4 and 5) is only noticeable in the first part of the plume and there is slight. The influence of D_o is likewise principally in the initial region but there it can be considerable (figure 6). The velocity in the contraction decreases with increasing D_o, while the distance of the virtual origin below the plane of injection increases ($Z_{virt} - Z_o$ = a few D_o). For the smaller D_o values, the predicted rate of contraction is too high for the results to be more than qualitatively reliable since the assumption of constant pressure in a cross-section is no longer admissable.

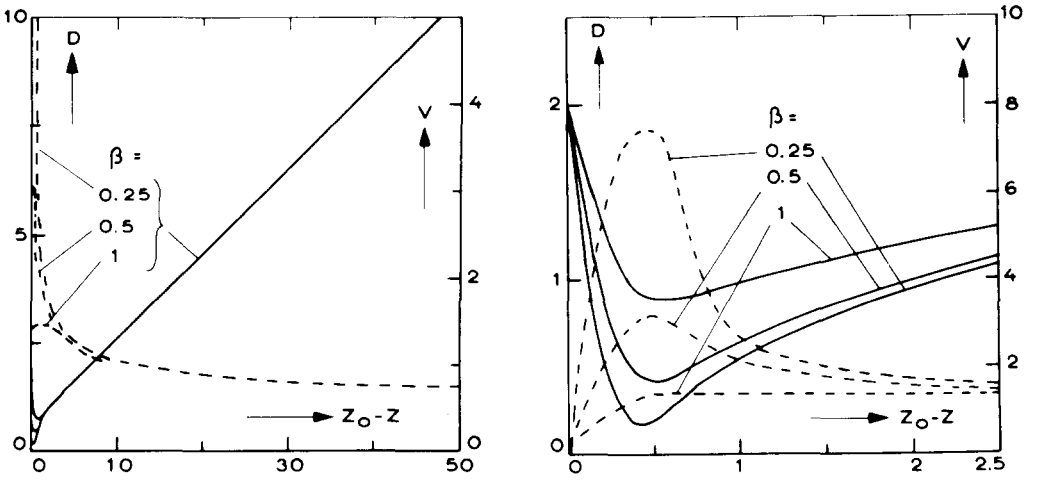

Figure 4. Influence of β value on plume development in the standard axisymmetric case (– D, — V).

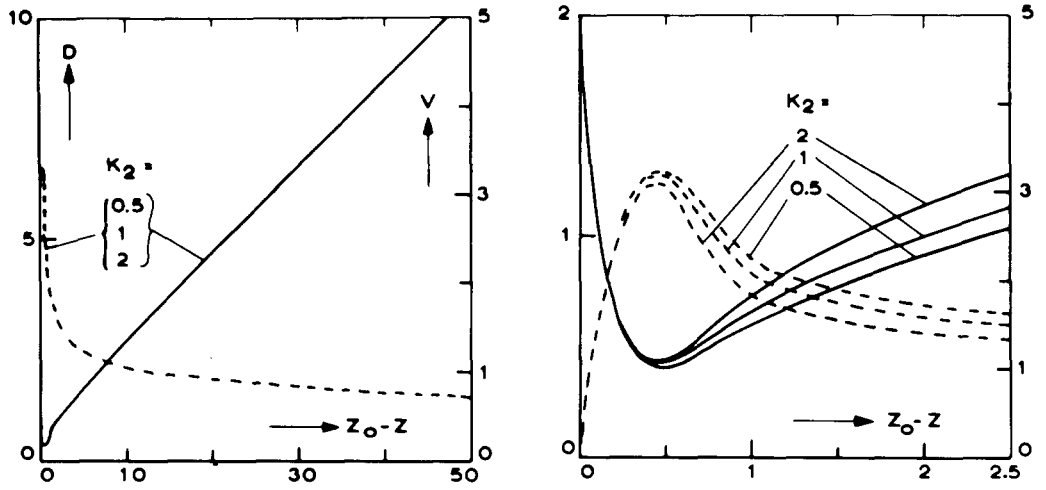

Figure 5. Influence of K_2 value on plume development in the standard axisymmetric case ($-D, --V$).

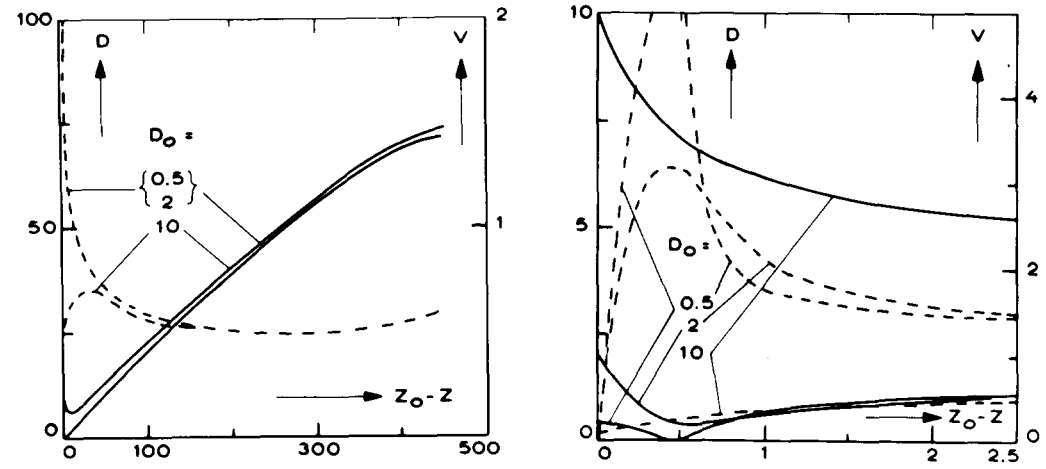

Figure 6. Influence of D_0 value on plume development in the standard axisymmetric case ($-D, --V$).

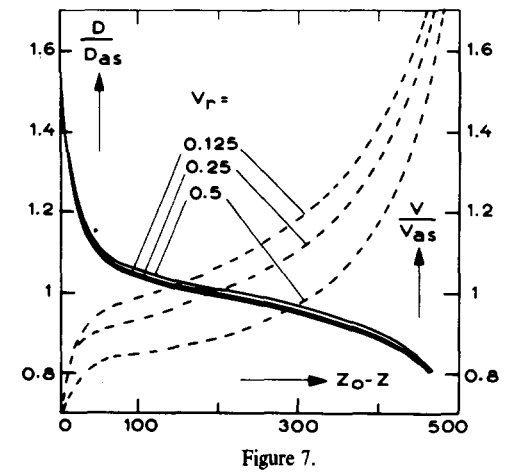

Figure 7.

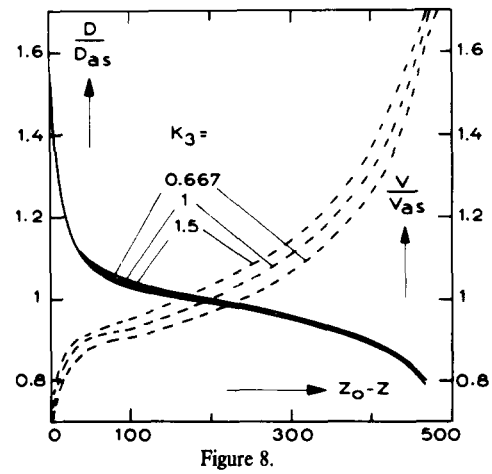

Figure 8.

Figure 7. Influence of V_r on the deviation from the asymptotic solution (D_{as}, V_{as}) in the standard axisymmetric case ($-D, --V$).

Figure 8. Influence of K_3 on the deviation from the asymptotic solution (D_{as}, V_{as}) in the standard axisymmetric case ($-D, --V$).

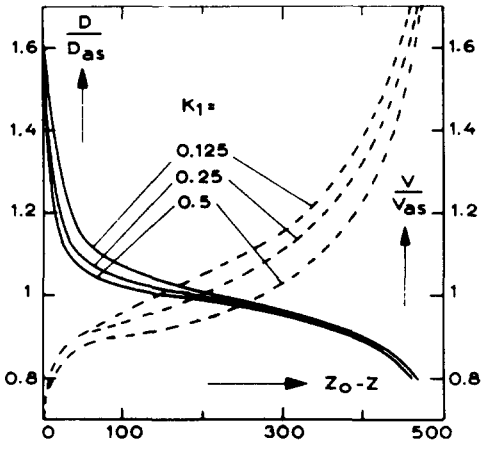

Figure 9.

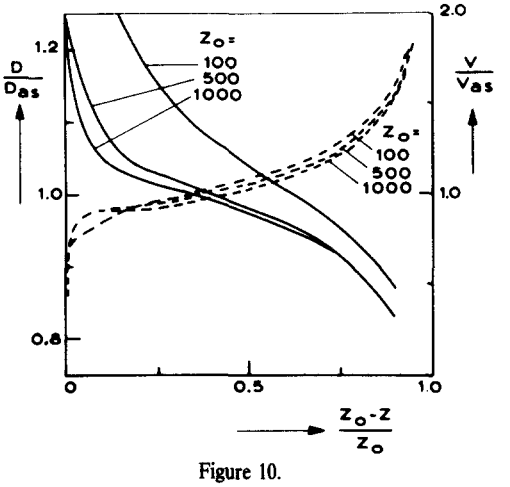

Figure 10.

Figure 9. Influence of K_1 on the deviation from the asymptotic solution (D_{as}, V_{as}) in the standard axisymmetric case (–D, – –V).

Figure 10. Influence of Z_o on the deviation from the asymptotic solution (D_{as}, V_{as}) in the standard axisymmetric case (–D, – –V).

The relation between the actual and the asymptotic solution for various values of V_r, K_3, K_1 and Z_o is indicated in figure 7–10.

The corresponding results for the standard† plane-symmetric case are given in figure 11.

5. EXPERIMENTAL RESULTS

5.1 *The system and the measurements*

The system employed is depicted in figure 12. A porous sintered-glass disc, of active diameter 26 mm, produced fairly uniform bubbles of equivalent diameter‡ about 2 mm (figure 13) in 28 cm of water in a 2.5 m diameter tank. Three flow rates were employed:

$$\text{Case 1, } G_o = 2.86 \times 10^{-5}\ \text{m}^3\,\text{s}^{-1}$$

$$\text{Case 2, } G_o = 2 \times (G_o)_{\text{case 1}}$$

$$\text{Case 3, } G_0 = 3 \times (G_o)_{\text{case 1}}.$$

At a flow rate of about 3.5 times that of case 1, the change in flow pattern alluded to in section 3 took place. The surface of the injector became completely covered in a layer of air from which large bubbles periodically broke away. From [40], it may therefore be concluded that

$$\frac{4K_2 \times (3.5 \times 2.84 \times 10^{-5})}{\pi(1 + K_3\beta)v_r} = (2.6 \times 10^{-2})^2.$$

If the standard values of section 4.2 are adopted for K_2, K_3 and β, this yields $v_r = 0.12\ \text{ms}^{-1}$: somewhat less than half the value measured higher up in the plumes. This agrees with Korbijn's (1977) conclusion that v_r is lower in the high-gas-fraction initial region of the plume.

Although the initial value of v_r may be expected to be somewhat higher in the lower flow rate cases 3, 2 and 1, for simplicity the term $4K_2/\pi(1 + K_3\beta)v_r$ will be assumed to have the same

†K_1' equal to 0.16, and the other parameters the same as in the standard axisymmetric case (table 2).
‡The diameter of a sphere of the same volume.

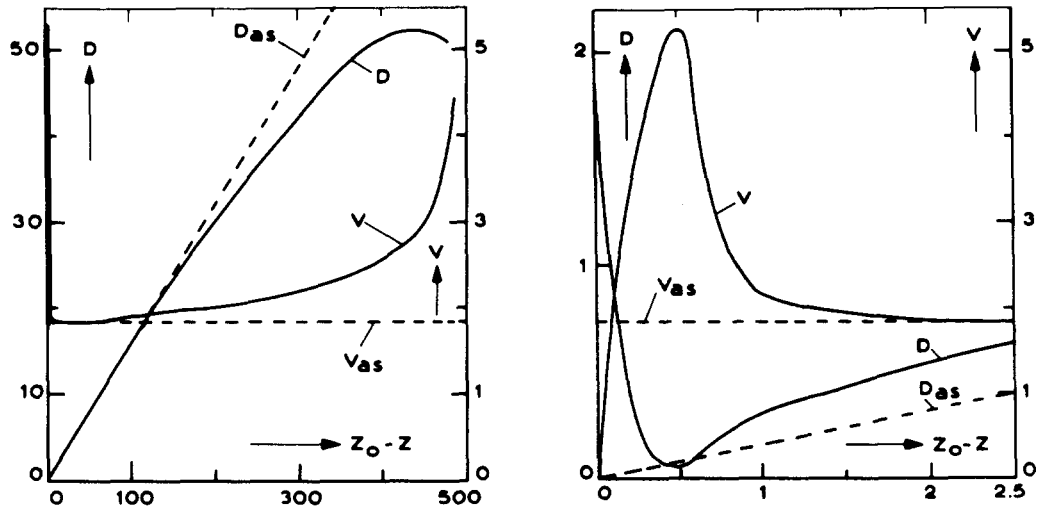

Figure 11. Variation of D and V with height in the standard plane-symmetric case (the broken lines indicate the asymptotic solution).

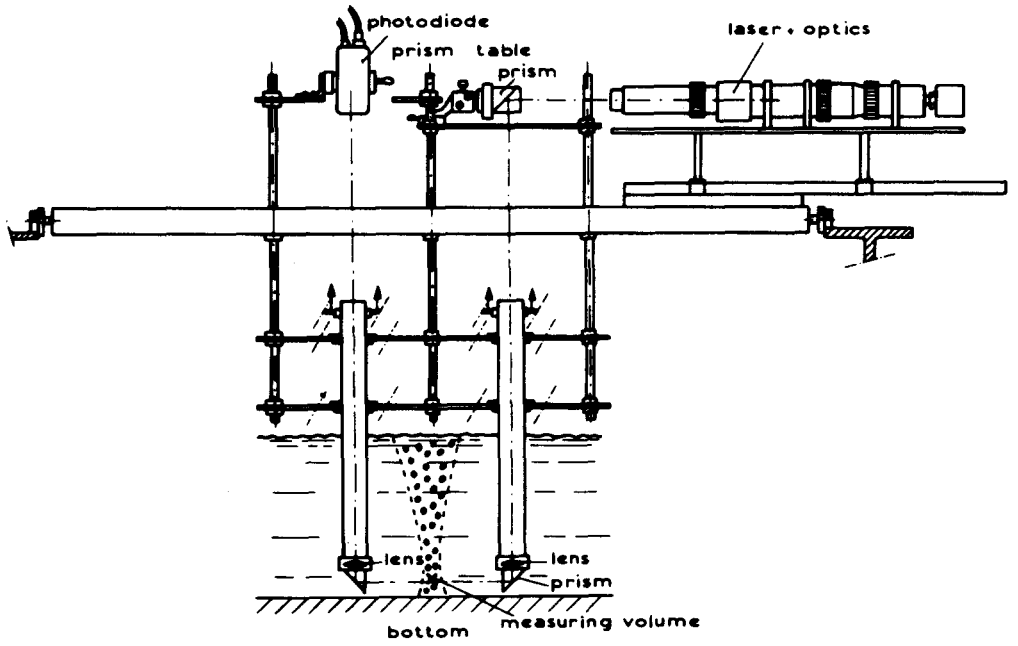

Figure 12. Experimental set-up.

value as at the transition flow rate. [40] then yields:

Case 1, $d_o \doteq 2.20$ cm
Case 2, $d_o = 1.70$ cm
Case 3, $d_o = 0.99$ cm.

The periscope system (figure 12) was used to carry out laser-doppler measurement of mean local liquid velocity, using the method of reference beam in forward scattering. The system was tested with an artificial beam interrupter, provided by a rotating disc, and found to measure correctly (Goossens 1979). These measurements were carried out in a number of cross sections of the plume in all three cases. Bubble velocity measurements were carried out in case 1 only, using the well-known double-electrode method (vertical electrode spacing about 4 mm).

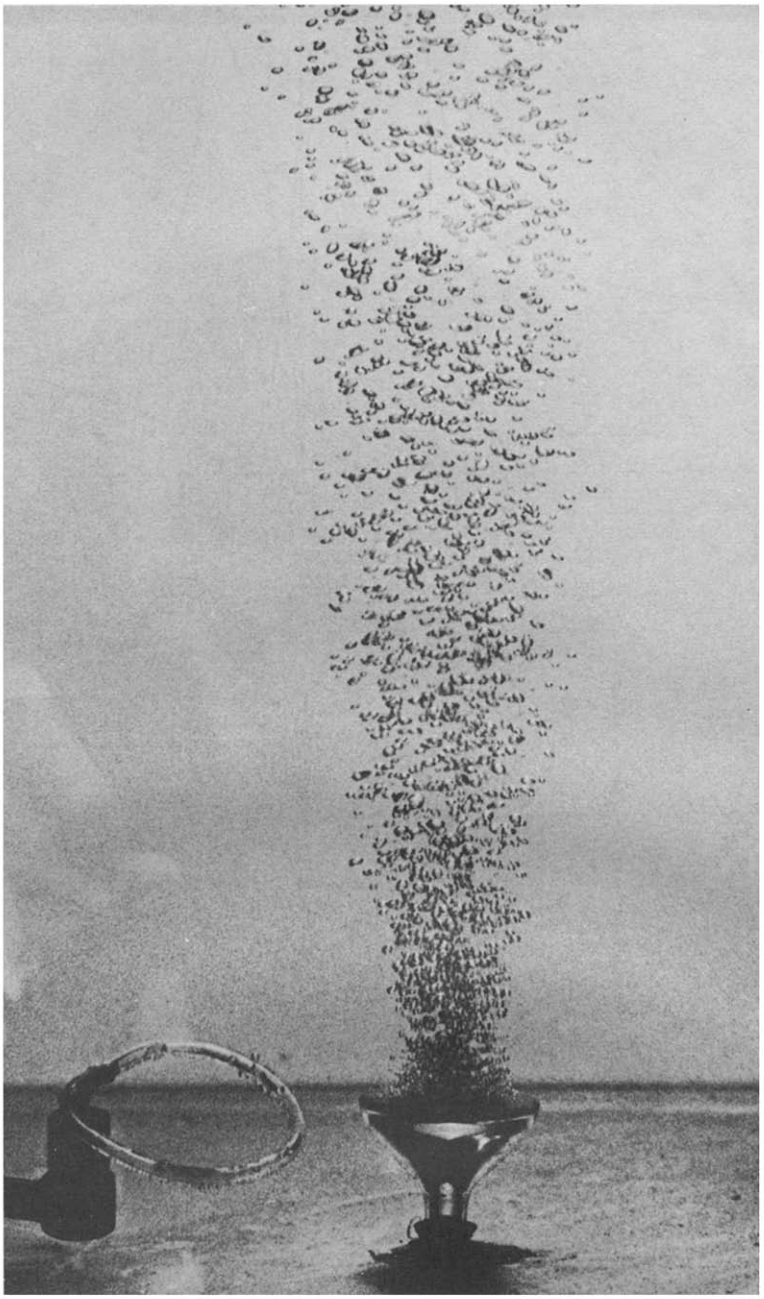

Figure 13. Bubble plume from a porous sintered-glass disc of active diameter 30 mm for a flow rate corresponding to case 1 ($G_o = 2.86 \times 10^{-5}$ m^3 s^{-1}).

5.2 *Results*

5.2.1 *Visual observations.* A photograph of a plume from a porous sintered glass disc under conditions similar to those of the measurements is shown in figure 13. The initial contraction is clearly observable.

5.2.2 *Liquid velocities.* As examples of the liquid velocity measurements, two profiles are presented in figure 14 for the lowest and highest gas flow rates (cases 1 and 3) at a height of some 12 cm above the injector. The profiles are normalized with the help of the maximum velocity, $\bar{u}_{max}$, and the half radius, $r_{1/2}$ (at which $\bar{u} = \bar{u}_{max}/2$). For comparison, a Gaussian profile is also shown. In both cases the correspondence with the Gaussian profile is very close up to a

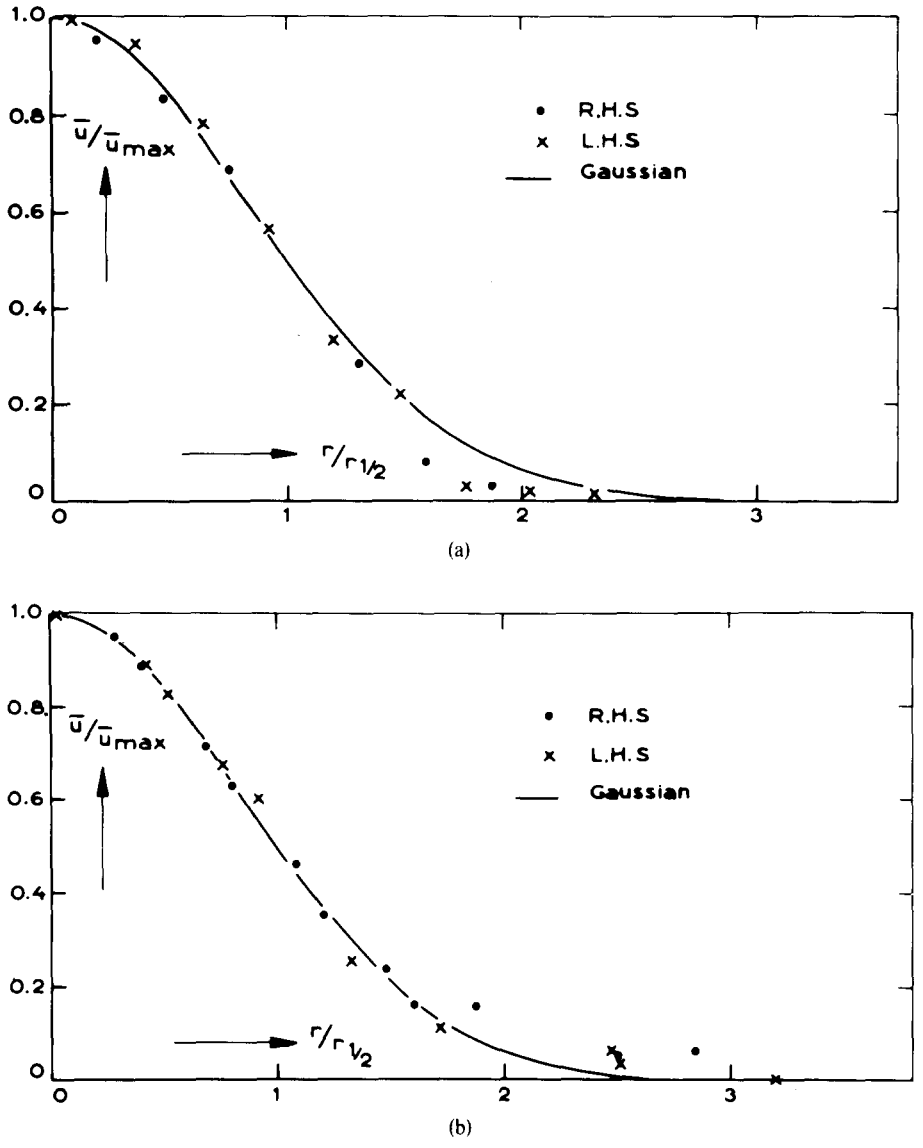

Figure 14. Variation of $\bar{u}$ across the plume for $z_0 - z \simeq 12$ cm: (a) case 1, (b) case 3.

normalized radius of 1.5. In case 1, no bubbles were found beyond this radius during the bubble-velocity or laser measurements, which presumably explains the low liquid velocities there. The reverse effect in case 3 is presumably due to the *presence* of bubbles in the outer flow (established by the laser measurements), as a result of the greater diffusing action of the liquid flow ($\bar{u}_{max}$ approximately double that in case 1).

5.2.3 *Bubble velocities.* Figure 15 shows the variation of relative bubble velocity (absolute velocity minus local liquid velocity) across the plume in the same situation as figure 14(a). The higher relative velocities in the outer zone of the plume could be explained by fact that the bubbles arriving here as a result of plume turbulence possess in general a higher axial component of velocity than the surrounding, bubble-free, entrained liquid.

The relative velocity of about 28 cm/s obtained in the central region of the plume agrees well with the free-rise velocity of bubbles of the size concerned (equivalent diameter about 2 mm) in pure water (figure 16). Although tap water was used in the experiment, it seems plausible that because of the rapid formation and high concentration of the bubbles, not enough surface-active matter diffuses to the bubbles in the plume to produce the tap-water characteristic.

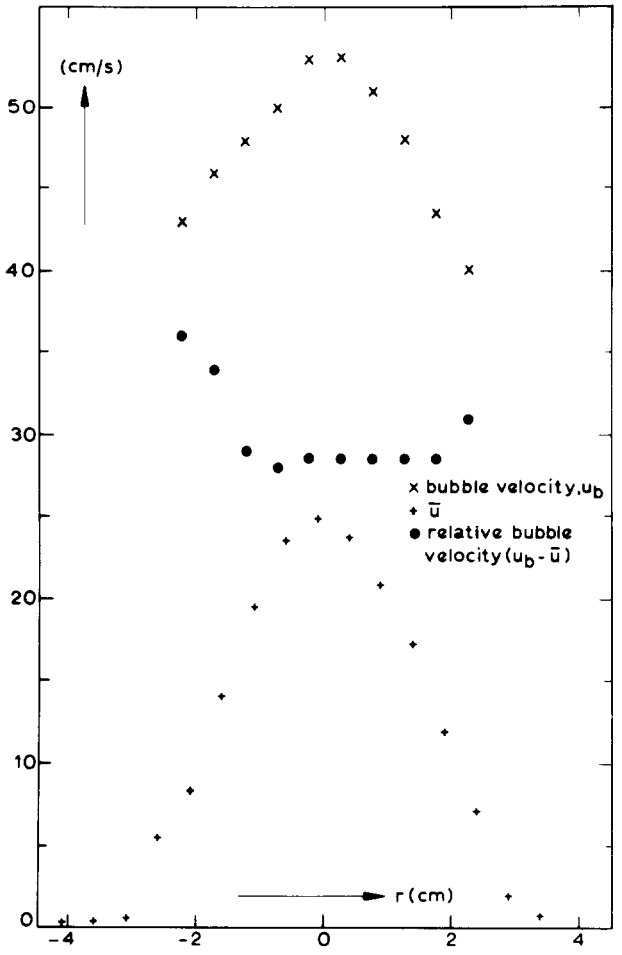

Figure 15. Variation of bubble velocity across the plume (case 1, $z_o - z = 12.1$ cm).

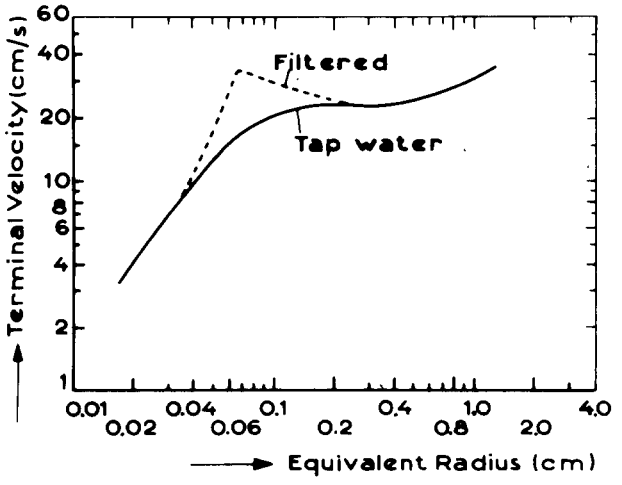

Figure 16. Rise velocities of bubbles in filtered and tap water (Haberman & Morton 1956).

5.2.4 *Mass entrainment rates.* Since the mean mass flux is given by

$$m = \rho \int_0^\infty 2\pi r(1-\alpha)(\bar{u}+\tilde{u})\,\mathrm{d}r = \rho \int_0^\infty 2\pi r(1-\alpha)\bar{u}\cdot\mathrm{d}r, \qquad [44]$$

the value of m, unlike that of M, can be obtained from the measured profiles of $\bar{u}$.

The correction required to take account of α in [44] is readily obtained (appendix 2) if the profiles of $\bar{u}$ and α are approximated as Gaussian as in [12] and [21]:

$$m/m_{\text{int}} = 1 - \alpha_{\max}/(1 + 1/\lambda^2) \quad [45]$$

with

$$\alpha_{\max} = \rho G/m_{\text{int}}[\lambda^2/(1+\lambda^2) + v_r\lambda^2/\bar{u}_{\max}], \quad [46]$$

where m_{int} is the mass flux obtained by integration of the velocity profiles without regard to α:

$$m_{\text{int}} = \rho \int_o^\infty 2\pi r\bar{u}\, dr. \quad [47]$$

The value of λ used is not of great importance since the magnitude of the correction proves insensitive to it. Here a value of unity is adopted since the boundary of the aerated zone, as revealed by the laser measurements, indicated λ to vary from somewhat less than unity in case 1 to somewhat greater in case 3.

The variation of the resulting values of m with height above the injector is shown in figures 17–19 together with the numerical predictions for various values of K_1, $v_r = 28$ cm/s and standard values of β, K_2 and K_3 (table 2). The choice of the latter value is discussed further in section 5.2.5. The correspondence between theory and measurement is good, especially in cases 1 and 2. The best-fit K_1 values are close to the single-phase value of 0.25, increasing somewhat with increasing gas flow rate.

5.2.5 *Momentum flux.* The momentum flux associated with the mean flow, $\bar{M}$ ([3]), can be calculated from the mean-velocity profiles, applying a similar correction for the gas fraction as in the case of the mass flux (appendix 2). At the same time the value of the total momentum flux, M ([1]), can be computed, based on the standard values of β, K_2 and K_3, $v_r = 28$ cm s^{-1} and the best-fit value for K_1 (see preceeding section). The results are given in table 3. In all cases $\bar{M}$ is considerably lower than M. The ratio $\bar{M}/M$ rises from as little as 40 per cent at the lowest measuring stations to as much as 80 per cent at the highest. Similar results are obtained if somewhat different values are used for the various parameters. This is illustrated in table 4,

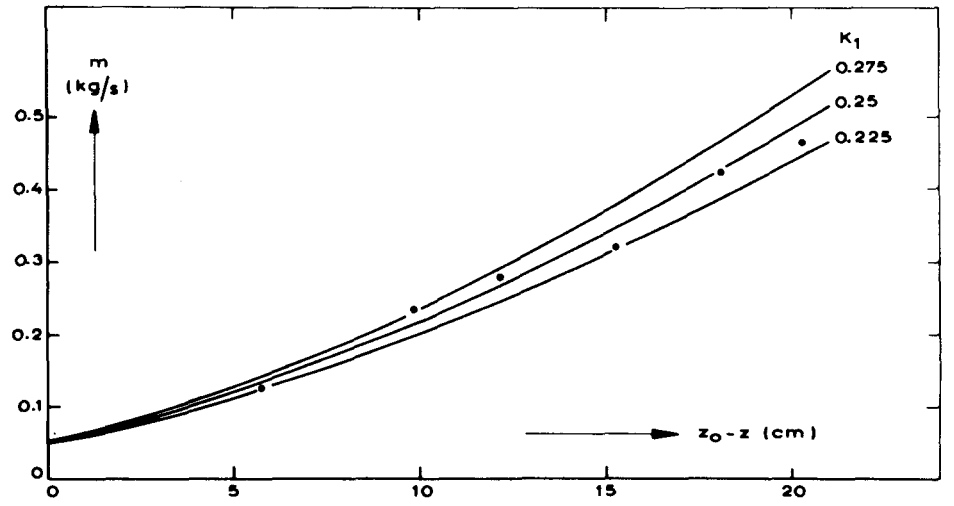

Figure 17. Measured and predicted variation of mass flux, m, with height (case 1).

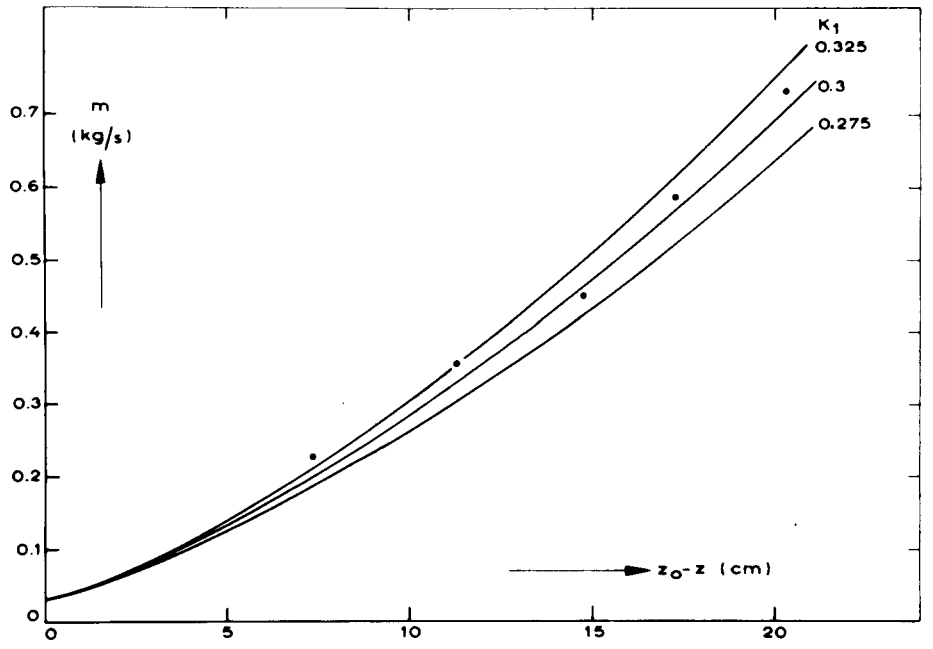

Figure 18. Measured and predicted variation of mass flux, m, with height (case 2).

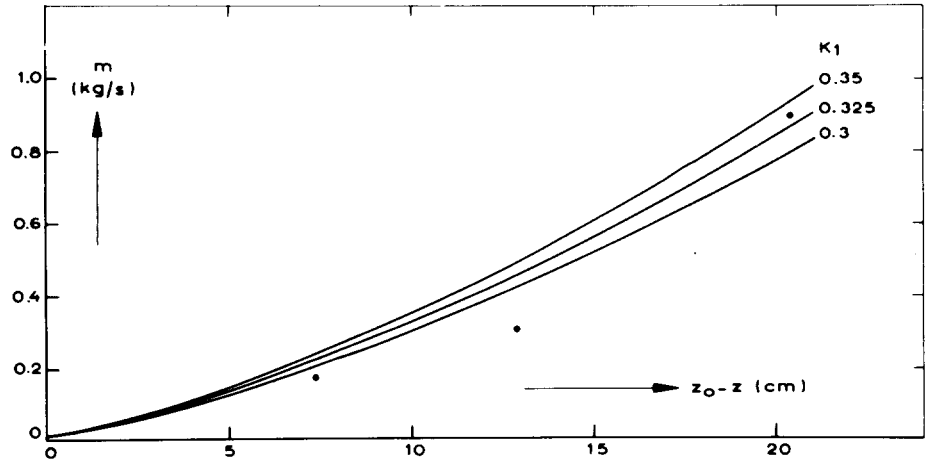

Figure 19. Measured and predicted variation of mass flux, m, with height (case 3).

where the value of M at a height of 14 cm above the injector is calculated in case 1, with the same values of the various parameters as above, except for the parameter cited in each case.

The increase in $\bar{M}/M$ with height suggests that the velocity fluctuations ($\tilde{u} \sim v_r$) produced by the relative motion of the bubbles are responsible for the large value of $\tilde{M}$ ([4]). In view of the composition of the terms $\bar{M}$ and $\tilde{M}$ ([1]–[4]), a measure of this effect may be expected to be $\alpha_{max}(v_r/\bar{u}_{max})^2$. This quantity is given in table 3 and is plotted against $\tilde{M}/M$ in figure 20. Although a good deal of scatter is present, the general upward trend of $\tilde{M}/M$ with decreasing $\alpha_{max}(v_r/\bar{u}_{max})^2$ is clearly observable, and no systematic separation of three cases occurs, despite the very different contributions of α_{max} and $(v_r/\bar{u}_{max})^2$ to the total term $\alpha_{max}(v_r/\bar{u}_{max})^2$.

In figure 21, $\bar{u}_{max}/2v$ is plotted against the same group. For a Gaussian profile of velocity with no velocity fluctuations, this quantity should be unity ([14]). The "too-low" measured values of $\bar{u}_{max}$ are clearly observable. Again the effect correlates with $\alpha_{max}(v_r/\bar{u}_{max})^2$, but now a systematic separation of the three cases is discernable, presumably due to the systematic

Table 3. Relation between M and $\bar{M}$

$z_o - z, m$	$\bar{M}$ kgms^{-2}	M kgms^{-2}	$\bar{M}/M$	α_{max}	$\alpha_{max}(v_r/\bar{u}_{max})^2$
case 1, $K_1 = 0.25$, $v_r = 0.28$ ms^{-1}, β, K_2 and K_3 standard					
0.0577	0.0145	0.038	0.38	0.12	0.183
0.0986	0.036	0.058	0.61	0.07	0.084
0.1216	0.042	0.070	0.60	0.06	0.076
0.1524	0.047	0.086	0.55	0.05	0.063
0.1809	0.062	0.101	0.61	0.04	0.046
0.2029	0.072	0.113	0.63	0.04	0.039
case 2, $K_1 = 0.3$, $v_r = 0.28$, β, K_2 and K_3 standard					
0.0734	0.050	0.069	0.73	0.19	0.094
0.1125	0.080	0.104	0.77	0.13	0.059
0.1474	0.098	0.137	0.71	0.10	0.046
0.1724	0.134	0.161	0.83	0.08	0.036
0.2029	0.144	0.192	0.75	0.07	0.032
case 3, $K_1 = 0.325$, $v_r = 0.28$, β, K_2 and K_3 standard					
0.0734	0.039	0.087	0.45	0.38	0.110
0.1283	0.066	0.157	0.42	0.22	0.079
0.2034	0.189	0.261	0.73	0.08	0.032

Table 4. Variation of M with the various parameters (case 1, 14 cm above the injector)

Parameter changed	M kgms^{-2}	$M/M_{reference}$
None	0.079	1
$v_r = 0.20$ ms^{-1}	0.083	1.05
$d_o = 0.015$ m	0.071	0.90
$\beta = 0.25$	0.071	0.90
$K_1 = 0.4$	0.087	1.10
$K_2 = 0.5$	0.079	1.00
$K_3 = 1.2$	0.074	0.94

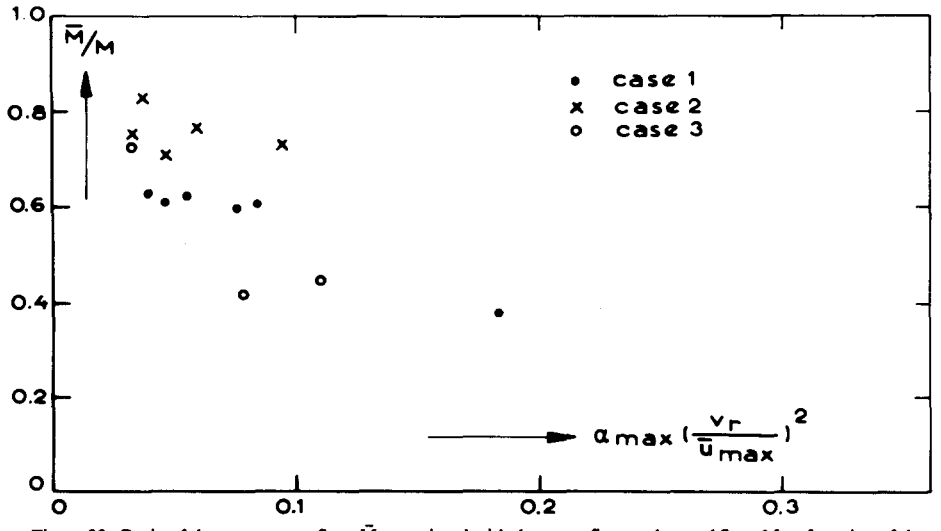

Figure 20. Ratio of the momentum flux, $\bar{M}$, associated with the mean flow to the total flux, M, as function of the bubble-influence parameter $\alpha_{max}(v_r/\bar{u}_{max})^2$.

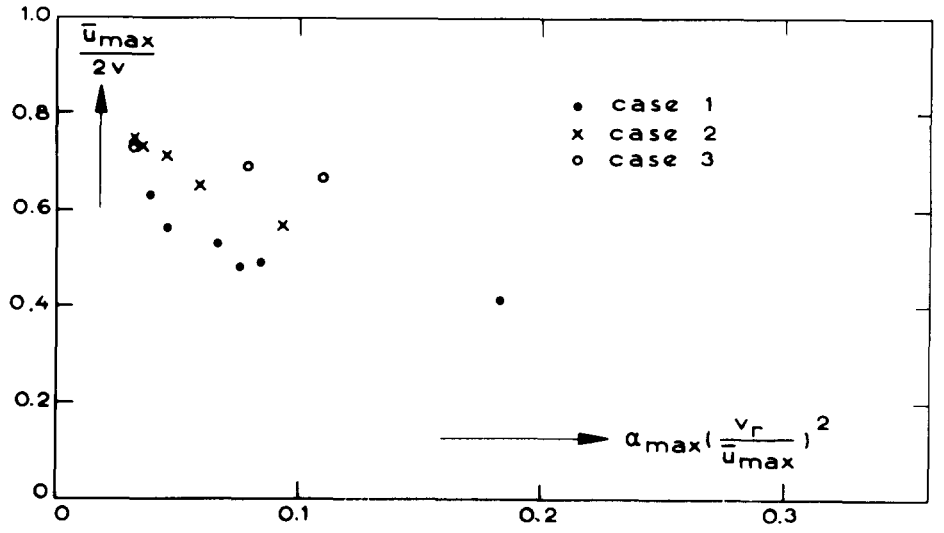

Figure 21. Ratio of $\bar{u}_{max}/2$ to the equivalent velocity, v as function of the bubble-influence parameter, $\alpha_{max}(v_r/\bar{u}_{max})^2$.

change in the shape of the velocity profile with increasing gas flow rate discussed in section 5.2.2.

The same phenomenon ("too-low" plume velocities) was remarked on by Cederwall and Ditmars and by Tekali and Maxwell in the context of plane-symmetric plumes. In the plane case, the effect may be expected to persist to greater heights because of the relatively slow decay of the gas fraction. Cederwall and Ditmars would also have found the effect in the axisymmetric case, however, had they taken $\lambda \sim 1$ rather than the unrealistically low value of 0·2.

CONCLUSIONS

(1) *Theoretical results*

(1.1) Simple equations for the evolution of buoyant two-phase plumes can be derived without assumptions as to the form of the velocity and gas-fraction profiles or as to the fraction of the momentum flux associated with the mean flow. The equations contain three dimensionless parameters K_1, K_2 and K_3 of which the orders of magnitude, but not the exact values, are known *a priori.*

(1.2) For extended sources, two stages may be distinguished in the evolution of the plume. In the first, only liquid in the immediate vicinity of the bubbles is in motion, while in the second the flow may be treated as a plume. Stage 1 normally has negligible height but serves to establish the initial conditions for stage 2.

(1.3) For typical values of the relevant parameters, plumes from extended sources first contract and then expand almost linearly (i.e. rate of change of equivalent diameter with height = a positive constant). The virtual origin of this expansion is a few initial equivalent diameters below the gas injection plane.

(1.4) The parameters of greatest influence on the plume development are the volume injection rate of gas and the acceleration due to gravity. Solutions of the plume equations normailized with length and velocity scales constructed from these parameters exhibit only a second-order dependence on the remaining parameters (figures 4–10), and so closely resemble the asymptotic solution for the single-phase, incompressible case.

(1.5) The greatest deviation from the asymptotic solution is a second contradiction, which is predicted to occur near the surface of very deep bodies of liquid as a reault of gas expansion in the final part of the plume.

(2) *Experimental results*

(2.1) The rates of mass entrainment in the small axisymmetric, air-tap water plumes investigated correspond to an entrainment coefficient K_1 equal to, or somewhat greater than, that for a single-phase jet or plume (0.25–0.33). For the system concerned, K_1 tends to increase with increasing gas injection rate.

(2.2) The measured profiles of mean liquid velocity can be closely approximated as Gaussian up to about $1.5r_{1/2}$ ($r_{1/2}$ the radius at which $\bar{u} = \bar{u}_{max}/2$). Beyond this point, liquid velocities are lower than Gaussian for the lowest gas injection rate and higher for the highest gas injection rate. This fact ties in with the absence of bubbles in the outer flow in the former case ($\lambda < 1$; [21]) and their presence in the latter ($\lambda > 1$).

(2.3) The relative bubble velocities in the core of the plume correspond well with free-rise velocities in *pure* water. In the outer flow, relative velocities are higher. These facts may be explained, respectively, by the large ratio of bubble surface to water volume within the plume and by the outer, bubble-containing liquid originating in the high-velocity core flow.

(2.4) The momentum flux associated with the mean liquid velocity, $\bar{M}$, can be as little as 40 per cent of the total momentum flux, M, predicted from the optimal value of K_1. This effect is attributed to the large contribution to M of velocity fluctuations associated with the bubbles. The ratio $\bar{M}/M$ correlates with the parameter $\alpha(v_r/\bar{u}_{max})^2$ and rises to around 80 per cent high in the plume, where this parameter is small. This effect offers an explanation of the "too-low" plume velocities found by other investigators.

REFERENCES

ABRAHAM, G. 1972 Theoretical consideration of salt-intrusion prevention in sluices by bubble curtains (in Dutch). *De Ingenieur* **84**, 9–17.

CEDERWALL, K. & DITMARS, J. D. 1970 Analysis of air-bubble plumes. California Inst. Tech. Rep. KH-R-24.

FREEDMAN, W. & DAVIDSON, J. F. 1969 Hold-up and liquid circulation in bubble columns. *Trans. Inst. Chem. Engrs* **47**, T 251–262.

GOOSSENS, L. H. J. & SMITH J. M. 1975 The hydrodynamics of unconstrained bubble columns for mixing lakes and reservoirs. *Chem. -Ing. Tech.* **47**, 951.

GOOSSENS, L. H. J. 1979 Reservoir destratification with bubble columns. Ph.D. Thesis, Delft University of Technology.

HABERMAN, W. L. & MORTON, R. K. 1956 An experimental study of bubbles moving in liquids. *ASCE Trans.* **121**, 227–250.

HUSSAIN, N. A. & SIEGEL, R. 1976 Liquid jet pumped by rising gas bubbles. *J. Fluid Engng ASME* **98**, 49–57.

KOBUS, H. 1973 *Bemessungsgrundlagen und Anwendungen für Luftschleier im Wasserbau.* E. Schmidt Verlag, Berlin.

KORBIJN, F. 1977 Behaviour of an air-water plume in the injection region (in Dutch). Kandidaats-Report, Lab. Physical Technology, Delft University of Technology.

RICOU, F. P. & SPALDING, D. B. 1961 Measurements of entrainment by axisymmetric turbulent jets. *J. Fluid Mech.* **11**, 21–23.

RIETEMA, K. & OTTENGRAF, S. P. P. 1970 Laminar liquid circulation and bubble street formation in a gas–liquid system. *Trans. Inst. Chem. Engrs* **48**, T54–62.

TEKELI, S. & MAXWELL, W. H. C. 1978 Behavior of air bubble screens. Univ. Illinois, Dept. Civ. Engng Rep. 33.

TURNER, J. S. 1969 Buoyant plumes and thermals. *Ann. Rev. Fluid Mech.* **1**, 29–44.

APPENDIX 1

Relation between general and Gaussian plume parameters for the low gas-fraction, negligible velocity-fluctuation case

Plume width and velocity. The expressions for m and M in the axisymmetric case reduce to

$$m = \rho \int_o^\infty 2\pi r u_{max}\, e^{-r^2/b^2} \cdot dr = \pi \rho u_{max} b^2 \qquad [A1.1]$$

$$M = \rho \int_o^\infty 2\pi r u_{max}^2\, e^{-2r^2/b^2} \cdot dr = \pi \rho u_{max}^2 b^2/2\,. \qquad [A1.2]$$

Substitution of [A1.1] and [A1.2] in [10] and [11] then yields [13] and [14].

In the plane-symmetric case,

$$u = u_{max}\, e^{-x^2/b^2}\,, \qquad [A1.3]$$

the corresponding results are:

$$m = 2\rho \int_o^\infty u_{max}\, e^{-x^2/b^2} \cdot dx = \rho u_{max}\, b\sqrt{\pi} \qquad [A1.4]$$

$$M = 2\rho \int_o^\infty u_{max}^2\, e^{-2x^2/b^2} \cdot dx = \rho u_{max}^2 b\sqrt{(\pi/2)} \qquad [A1.5]$$

and

$$d = \sqrt{(2\pi)}b\,, \quad v = u_{max}/\sqrt{2}\,. \qquad [A1.6]\,,\,[A1.7]$$

Gas distribution parameter. The volume flux of gas through any section of the plume, G, is given in the axisymmetric case by

$$G = \int_o^\infty 2\pi r(u + v_r)\alpha\, dr$$

$$= \int_o^\infty 2\pi r(v_r + u_{max}\, e^{-r^2/b^2})\alpha_{max}\, e^{-r^2/(\lambda b)^2} \cdot dr$$

$$= \pi v_r \alpha_{max}(\lambda b)^2 + \pi u_{max}\alpha_{max}(\lambda b)^2/(1+\lambda^2)\,. \qquad [A1.8]$$

The sectional area occupied by gas, a, is given by

$$a = \int_o^\infty 2\pi r\alpha \cdot dr = \pi \alpha_{max}(\lambda b)^2\,. \qquad [A1.9]$$

Substitution of [A1.8] and [A1.9] in [23], bearing in mind that

$$G = G_o z_o/z \qquad [A1.10]$$

and making use of [14], yields [22].

In the plane-symmetric case, the corresponding results are:

$$G = v_r \alpha_{max}(\lambda b)\sqrt{\pi} + u_{max}\alpha_{max}(\lambda b)\sqrt{[\pi/(1+\lambda^2)]} \qquad [A1.11]$$

$$a = \alpha_{max}(\lambda b)\sqrt{\pi} \qquad [A1.12]$$

$$K_3' = \sqrt{[2/(1+\lambda^2)]}\,. \qquad [A1.13]$$

APPENDIX 2

Corrections to the integrated profiles of $\bar{u}$ and $\bar{u}^2$ to take account of absence of liquid during a fraction of the time

Only the axisymmetric case is considered here. From [44] and [41], the relation between m and m_{int} is

$$m/m_{int} = \int_o^\infty 2\pi r(1-\alpha)\bar{u} \cdot dr / \int_o^\infty 2\pi r\bar{u} \cdot dr. \qquad [A2.1]$$

If the profiles of $\bar{u}$ and α are approximated as Gaussian ([12] and [21]), [A2.1] yields [45].

The magnitude of α_{max} is obtained from the ratio of G and m_{int}/ρ:

$$\frac{G}{(m_{int}/\rho)} = \frac{\int_o^\infty 2\pi r(\bar{u}+v_r)\alpha \cdot dr}{\int^\infty 2\pi r\bar{u} \cdot dr}$$

$$= \frac{\alpha_{max}\lambda^2}{1+\lambda^2} + \frac{v_r\alpha_{max}\lambda^2}{u_{max}},$$

which yields [46].

The relation between $\bar{M}$ and $\bar{M}_{int}$ is

$$\bar{M}/\bar{M}_{int} = \int_o^\infty 2\pi r(1-\alpha)\bar{u}^2 \cdot dr / \int_o^\infty 2\pi r\bar{u}^2 \cdot dr$$

$$= 1 - \alpha_{max}/(1 + 1/2\lambda^2). \qquad [A2.2]$$